

Stenting-Induced Vasa Vasorum Compression and Subsequent Flow Resistance: a Finite Element Study

Andrea Corti (1), Annalisa De Paolis, PhD (1), John Tarbell, PhD (1), Luis Cardoso, PhD (1)

¹The City College of New York, Department of Biomedical Engineering, Steinman Hall, 160 Convent Ave, New York, NY 10031, Tel: (212) 650-7154, Fax: (212) 650-6727.

Corresponding author: Luis Cardoso, PhD, Cardoso@ccny.cuny.edu

Funding

This research was supported by NIH grants 1R01HL136431, 1SC1DK103362, NSF grants CMMI-1662970, CMMI-1333560, MRI-0723027, MRI-1229449.

Acknowledgment

We thank Prof Fergal Boyle and Dr Eoin Murphy from the Dublin Institute of Technology for providing part of the stent designs considered in this study. Their help was critical for the completeness of this study.

Abstract

Vascular stenting is a common intervention for the treatment of atherosclerotic plaques. However, stenting still has a significant rate of re-stenosis caused by Neointimal Hyperplasia (NH) formation. In this study, we evaluate whether stent overexpansion leads to Vasa Vasorum (VV) compression, which may contribute to vascular wall hypoxia and restenosis. An idealized multi-layered fibroatheroma model including Vasa Vasorum was expanded by three coronary stent designs up to a 1.3:1 stent/artery luminal diameter ratio (exp1.1, exp1.2, exp1.3) using a finite element analysis approach. Following Poiseuille's law for elliptical sections, the fold-increase in flow resistance was calculated based on VV compression in the Intima (Int), Media (Med) and Adventitia (Adv). The VV beneath the plaque experience the smallest degree of compression, while the opposite wall regions are highly affected by stent over-expansion. The highest compressions for Adv, Med and Int at exp1.1 are 60.7, 65.9, 72.3%, at exp 1.2 are 62.1, 67.3, 73.5% and at exp 1.3 are 63.2, 68.7, 74.8%. The consequent fold-increase in resistance to flow for Adv, Med and Int at exp1.1 are 3.3, 4.4, 6.6, at exp1.2 are 3.5, 4.7, 7.2 and at exp1.3 are 3.8, 5.1, 7.9. Stent over-expansion induces significant VV compression, especially in the Intima and Media layers, in agreement with previously observed Media necrosis and loss in elasticity after stenting. The observed steep increase in flow resistance suggests the blood flow and associated oxygen delivery would drop up to five times in the Media and almost eight in the Intima, which may lead to neointimal hyperplasia and restenosis.

Keywords:

Vascular stenting, neointimal hyperplasia, restenosis, vasa vasorum, vascular wall hypoxia, finite element analysis

1 Introduction

2 Vascular disorders represent the principal cause of death in Western Countries (Benjamin et al.
3 2018),(Benjamin et al. 2019). Atherosclerotic disease, the underlying cause of heart attacks and stroke, is
4 initiated by cholesterol build-up beneath the endothelium, which ultimately evolves into a lipid plaque, known
5 as fibroatheroma. Currently, the most reliable treatment for symptomatic vascular narrowing is Percutaneous
6 Transluminal Angioplasty (PTA), which widens the narrowed sections of the artery using a catheter balloon and
7 often placing a medical stent, a slender, expandable, cylindrical metal mesh in the region of vascular occlusion
8 (Meads et al. 2000). The stent works as a mechanical support for the vascular wall, re-opening the pathological
9 region and restoring the original blood flow. However, PTA with stenting is often complicated by in-stent
10 restenosis (ISR). ISR is the result of excessive tissue formation around the stent, referred to as Neointimal
11 Hyperplasia (NH), which may result in the failure of the implant. Although ISR is linked to different aspects of
12 the procedure, recent studies have highlighted the relationship between reduced levels of oxygen tension within
13 the stented artery wall and NH formation (Caro et al. 2013; Cheema et al. 2006; Murphy et al. 2016; Santilli,
14 Tretinyak, and Lee 2000; Tarbell et al. 2020; Tretinyak et al. 2002). The stent itself plays a key role in
15 determining the overall oxygen supply to the underlying tissue. Even though the stent restores the required blood
16 flow to downstream vasculature, it may induce a hypoxic condition for the arterial layers around its structure.
17 On one hand, the shape of the stent struts influences the local hemodynamics and oxygen transport rates from
18 the blood vessel lumen. Blood flow disturbance in the near wall region around the stent struts results in a reduced
19 oxygen flux through the inner lining of the vascular wall that affects oxygen tension in the intima and inner
20 media layers of the vessel wall (Murphy et al. 2016). On the other hand, the mechanical expansion of the device
21 seems to influence oxygen tensions in the outer vascular layers, perfused by supplementary capillary networks
22 known as Vasa Vasorum (VV) (Santilli, Tretinyak, and Lee 2000),(Sanada et al. 1998).

23 Vasa Vasorum represent the main source of oxygen for the outer Media and Adventitia layers, areas that are
24 beyond the reach of oxygen diffusion from the lumen. In the case of atherosclerosis, these microvessels can grow
25 down into the intimal layer, as a result of the oxygen deficiency caused by the fibroatheroma (Cheema et al.
26 2006), (Pels et al. 1999), (Vasuri et al. 2012). Depending on their origin, VV are divided into three categories
27 (Ritman and Leman 2008): Vasa Vasorum Interna VVI, when the origin is the main lumen itself and the
28 branching network remains inside the arterial wall; Vasa Vasorum Externa VVE, when the origin is located
29 outside the vascular wall and comes from a major branch emerging from the main lumen; Venous Vasa Vasorum
30 VVV, when the tree structure starts from a neighbouring vein. In the present study, we have considered a Vasa
31 Vasorum geometry that could represent either VVE or VVV, as its “mother branch” originates from outside the
32 vascular wall.

33 Previous research has focused its attention on understanding the effect of disruption of blood flow through
34 Vasa Vasorum (Kantor and Möhlenkamp 2003; Sanada et al. 1998; Vasuri et al. 2012). The results are often
35 medial necrosis, stagnant interstitial fluid, decreased vascular wall nutrition, and wall hypoxia. All of these may
36 occur when the artery is stent-expanded. Stent-expanded arteries may reach sufficiently elevated degrees of
37 deformation such that high circumferential and radial stresses (stretches) could compress VV thus diminishing
38 blood flow through VV and reducing oxygen delivery to the outer layers of the vessel wall. During stent
39 expansion, circumferential stresses in the layers remain rather small as long as the elastic fibres are able to
40 stretch. Once they reach the maximum extension, the stress begins to increase exponentially as collagen, which
41 is 100 to 1,000 times stiffer than elastin, bears increasing load (Fratzl 2008). On the other hand, radial stress is
42 the compressive component responsible for squeezing the structures in the artery wall. Increments in both
43 circumferential and radial stresses likely affect the original VV morphology and may contribute to artery wall
44 hypoxia. This mechanism naturally implies a relation between final stent expansion ratio, arterial stress and VV
45 compression that could provide the link between transarterial wall oxygen gradient and the degree of stent

1 expansion (Santilli, Tretinyak, and Lee 2000), (Ritman and Leman 2008). In clinical practice, stents are routinely
2 expanded under fluoroscopy to achieve a stent/artery luminal diameter ratio of 1.1:1. However, it is common
3 practice to further expand the stent with a second, less compliant balloon that is slightly shorter than the stent
4 itself. This step is referred to as stent post-dilation and it is performed to decrease the dog-boning effect (Fröbert
5 et al. 2013; Zhang et al. 2010). Even though post-dilation ensures a more uniform deformation of the stent, it
6 leads to a situation of overexpansion, where the ratio is 1.2:1 or greater (de Quadros et al. 2006). The overarching
7 hypothesis of this work is that stent expansion may compress the Vasa Vasorum, resulting in reduction of
8 vascular wall blood perfusion leading to wall hypoxia. Previous studies have used Finite Element Analysis (FEA)
9 to investigate the mechanical interaction between expanded stents and atherosclerotic tissues (Kantor and
10 Möhlenkamp 2003), (Fratzl 2008), (Zahedmanesh and Lally 2009), (Zhang et al. 2010). Others have focused on
11 the influence of the implant design over the hemodynamics and oxygen transport rates through the stented
12 lumen (Murphy et al. 2016), (L. Ritman, A. Lerman 2008). However, to our knowledge, there is no literature of
13 FEA exploring Vasa Vasorum compression induced by PTA assessing whether the final stent diameter could
14 induce a hypoxic situation in the outer vascular layers.
15

16 **Material and methods**

17 To assess the effect of stenting on Vasa Vasorum compression, we tested, using Finite Element Analysis
18 (Abaqus/CAE, Dassault Systemes, v.6.14-2), an idealized multi-layered fibroatheroma model (SolidWorks,
19 Dassault Systemes, v.2016), under three degrees of stent expansion. The atherosclerotic artery geometry
20 comprises the vascular layers Intima, Media, and Adventitia modelled as thick walled non-linear elastic
21 cylindrical tubes. The stenotic plaque consists of an atheroma cap and a lipid core placed in the intimal layer,
22 causing a moderately-severe lumen reduction. The geometry of the Vasa Vasorum comprises twelve capillary
23 network trees, each with three branches of decreasing diameter in both the axial and circumferential direction
24 that penetrates into each vascular layer and all around the artery. Our VV design is based on the graphical
25 illustration reported by (Vasuri et al. 2012). The artery is expanded by three different bare metal stents that are
26 first deployed at an expansion ratio of 1.1:1 and then post-dilated up to a ratio of 1.3:1. Deformation of the VV
27 produced by the different stents is quantified for each network tree by branch, layer, direction and location with
28 the artery, under the three expansion ratios. Analysis of such network is considered to cover most possible VV
29 locations within the artery. Vasa Vasorum deformation is then used to compute the increase in hydraulic
30 resistance on each Vasa due to stenting overexpansion.

31 **Model geometry and mesh**

32 The artery geometry presented in this study (Cardoso, L. *et al.* 2014) represents a 30 mm long vessel with
33 external diameter of 4 mm. The three vascular layers Intima, Media and Adventitia are modelled as straight
34 concentric cylindrical tubes with thickness values of 0.2, 0.2 and 0.4 mm respectively. The stenotic atheroma
35 cap has a thickness of 0.2 mm and results from a semi-annular lipid core localized inside the Intima, at the middle
36 of the artery section. The plaque causes a 60% occlusion of the lumen, defined as the ratio between the cross-
37 section area at the location of minimal radius in the stenosis and the cross-section area in the healthy region of
38 the vessel [Figure 1a]. The Vasa Vasorum geometry has an idealized anatomical layout and hierarchical
39 branching structure that has been described previously (Vasuri et al. 2012),(Ritman and Leman 2008),(H. M.
40 Kwon et al. 1998),(Williams and Heistad 1996). It comprises four main vessel trees that are concentric with the
41 artery, and located on the opposite side of the plaque (top), on the right and left sides and underneath the plaque,
42 as shown in [Figure 1b]. Each of these ‘mother’ vessels presents three descending branches that penetrate
43 longitudinally inside the arterial wall. These branches were classified as VV1, VV2 and VV3 accordingly to its
44 proximal to distal position within the artery [Figure 1a,b]. In addition, VV1, VV2 and VV3 have circumferential

1 branches, also shown in [Figure 1b]. The entire Vasa network is displayed under different perspectives in
2 [Figure 1a, b] and further described in [Table 1]. As illustrated, the entire structure of each Vasa has three
3 branches of decreasing diameter as it grows down towards the Intima. The geometry was designed such that the
4 branching site is at the middle position in each artery layer.

5

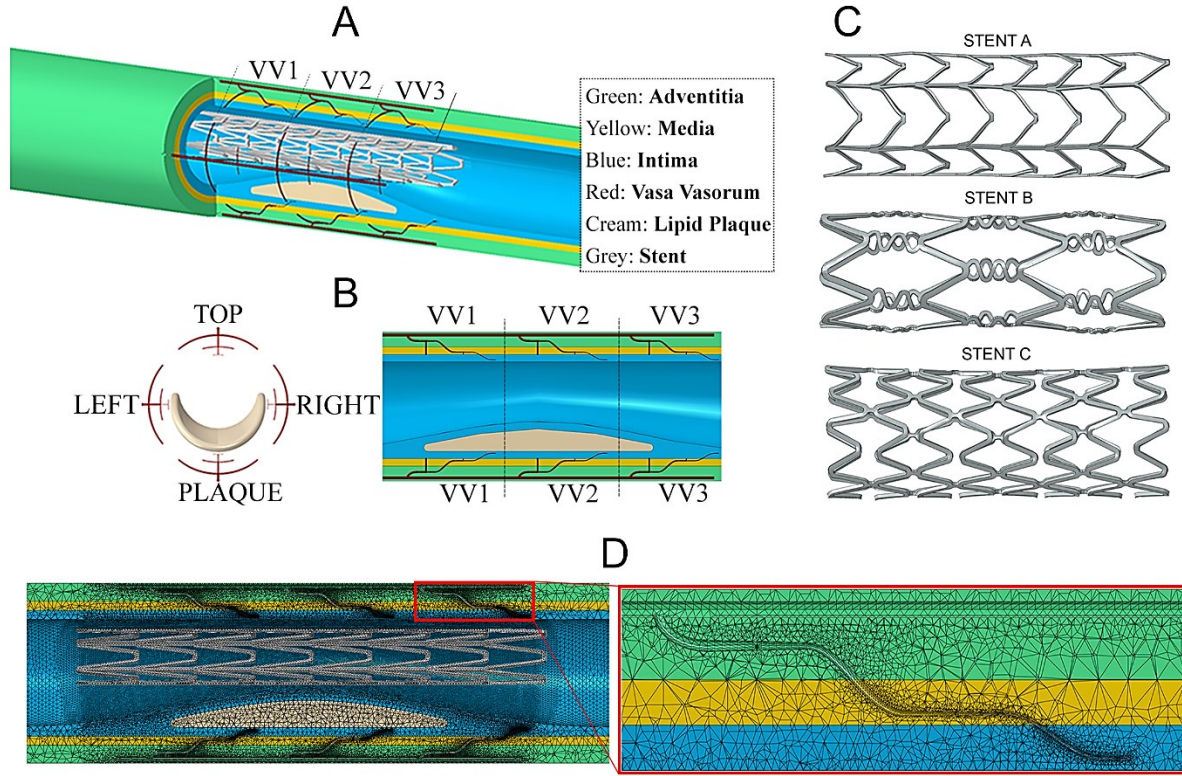
Table 1. Size of Vasa branches diameters in each arterial layer.

Layer	Main Branch Diameter (μm)	Longitudinal Branch Diameter (μm)	Circumferential Branch Diameter (μm)
Adventitia	70	40	30
Media	/	20	15
Intima	/	8	6

6

7 The three stent geometries resemble common designs from major medical companies, with different
8 geometrical features listed in [Table 2]. Stent A resembles the Thin-strut Multilink RX Ultra stent (Abbott
9 Laboratories, North Chicago, IL, USA), stent B represents the BX Velocity stent (Cordis of Johnson & Johnson,
10 Fremont, CA, USA) and stent C exemplifies the S7 AVE stent (Medtronic, Fridley, MN, USA) [Figure 1c].
11 These geometries were also considered since their performance on luminal oxygen transport has been previously
12 investigated (Murphy et al. 2016). A four-node linear tetrahedron and hybrid formulation (ABAQUS element
13 type C3D4H) was used to mesh the atherosclerotic artery. The three vascular layers have different element sizes,
14 with increasing mesh elements for outer regions. Moreover, central parts-corresponding to the pathological area
15 were meshed with finer elements compared to distal regions. This strategy allowed us to preserve accuracy in
16 the region of interest and reduce the number of elements where the same precision is not required. The same
17 mesh element type was used for the lipid core and stents. The atherosclerotic artery comprised more than 2
18 million elements. An illustration of the different mesh sizes can be observed in [Figure 1d].

19



1
2 **Figure 1.** Assembly of atherosclerotic artery, (A) Vasa Vasorum branches and stent A. (B) Vasa Vasorum network organization in
3 longitudinal and frontal view. (C) Stent A, B and C in their final expanded configuration. (D) Mesh assignment of the assembly,
4 with magnification of one Vasa branch.

Table 2. Design and dimensions of stents features.

Stent	Link configuration	Length (mm)	Strut thickness (mm)	Strut width (mm)
A	Peak-to-valley	10.65	0.07	0.10
B	Peak-to-peak	10.47	0.14	0.13
C	Peak-to-peak	7.93	0.10	0.10

5
6 **Material properties**

7 The arterial layers tissue properties were defined by the Holzapfel-Gasser-Ogden HGO constitutive model
8 (Holzapfel 2002),(Gasser, Ogden, and Holzapfel 2006), which adequately describes the nonlinear stress-strain
9 relationship of biological materials (Karimi, Navidbakhsh, and Razaghi 2014),(Cardoso, L. *et al.* 2014),(Lally,
10 Reid, and Prendergast 2004),(Karimi et al. 2014). This model considers the artery as an anisotropic material,
11 taking into consideration the collagenous fibre orientations in the layers. The HGO model describes the material
12 response to large deformation using the strain energy function given by (1):

13
$$\Psi = C_{10}(\bar{I}_1 - 3) + \frac{k_1}{2k_2} \sum_{i=1}^N [\exp(k_2 \langle \bar{E}_i^2 \rangle) - 1] + \frac{1}{D} \left(\frac{J^2 - 1}{2} - \ln J \right) \quad (1)$$

14 with,

15
$$\bar{E}_i \stackrel{\text{def}}{=} \kappa(\bar{I}_1 - 3) + (1 - 3\kappa)(\bar{I}_{4i} - 1), \quad (2)$$

1 where C_{10} describes the isotropic behaviour of the non-collagenous matrix of the artery and is related to the shear
 2 modulus μ of each layer by (3):

$$3 \quad C_{10} = \frac{\mu}{2}, \quad (3)$$

4 D is a material constant related to the bulk modulus K of the tissue by (4):

$$5 \quad D = \frac{K}{2}, \quad (4)$$

6 k_1 and k_2 are constants defining the anisotropic nature of the vascular tissue; the parameter κ describes the level
 7 of dispersion in the fibre direction; \bar{I}_1 is the first deviatoric strain invariant; J is the elastic volume ratio and
 8 $\bar{I}_{4i} = A_{0i} : \bar{C}$, $A_{0i} = a_{0i} \otimes a_{0i}$ are the invariants of the distortional part of the right Cauchy-Green strain \bar{C} . Since
 9 the collagen fibres are arranged in symmetrical spirals at different angles depending on the considered layer,
 10 they are expressed in a cylindrical coordinate system by (5):

$$11 \quad a_{0i} = \begin{bmatrix} 0 \\ \cos \beta_i \\ \sin \beta_i \end{bmatrix}, \quad i = 1, 2 \text{ fiber families} \quad (5)$$

12 where β_i are the directions of two ($i = 1, 2$) fibre families in the reference configuration, in each of the vascular
 13 layers.

14 Prior to the development of the HGO constitutive model, Holzapfel et al., 2005 developed another model
 15 that also takes into account the direction and dispersion of fibers in each artery layer. A complete set of
 16 coefficients was obtained for that model from experiments performed in separated artery layers of human
 17 coronary vessels. Unfortunately, no such dataset has been reported for the HGO model. To obtain the equivalent
 18 coefficients for the HGO model, we first recreated the average stress-strain curves for the Holzapfel et al., 2005
 19 model using the experimental mean values of stiffness μ , fibers orientation angle β and the fibers dispersion
 20 parameter ρ , while adjusting k_1 and k_2 to replicate the ultimate stretch and stress to rupture reported for each
 21 layer. Then, the HGO coefficients for each artery layer were obtained by curve fitting the average experimental
 22 stress-strain curves from Holzapfel et al., 2005 with the HGO model, where the stiffness μ , the fibers angle φ
 23 and the fibers dispersion parameter κ , were kept as reported in Holzapfel et al., 2005, and only the k_1 and k_2
 24 parameters were adjusted by minimizing the squared error between the data and the HGO model. The layer-
 25 specific values obtained for each hyperelastic material coefficient of the HGO model are listed in **[Table 3]**. The
 26 hypocellular lipid core is described by the first-order Ogden hyperelastic model given by (6):

$$27 \quad \Psi = \frac{2\mu}{\alpha^2} (\bar{\lambda}_1^\alpha + \bar{\lambda}_2^\alpha + \bar{\lambda}_3^\alpha) + \frac{1}{D} (J - 1)^2 \quad (6)$$

28 where the exponent α is a material parameter and λ_1, λ_2 and λ_3 are the principal stretches. Thus, the lipid core
 29 is considered as a homogeneous, isotropic, material - almost incompressible with the constants values reported
 30 in (He et al. 2020) **[Table 3]**. The stents have been made of Stainless Steel 316L with mechanical parameters
 31 reported in **[Table 3]** (Shit, Dhar, and Acharyya 2013).

32

33

34

35

Table 3. Material coefficients for the arterial layers, considered as anisotropic hyperplastic; lipid core, considered as linear elastic; stent, considered as metallic.

Layer	C_{10} (kPa)	D	k_1 (kPa)	k_2 (--)	κ	β_i (degrees)
Adventitia	3.78	0	1.99	6.36	0.15	67.0
Media	0.65	0	184.7	17.13	0.25	20.61
Intima	13.95	0	53.72	2.66	0.163	60.3
Element	μ (kPa)	D	α	Density (kg/ m ³)		
Lipid Core	3.968	0.239019	13.8367	1.22		
	Young's Modulus E (GPa)	Poisson's Ratio	Tangent Modulus (MPa)	Density (kg/m ³)		
Stent	196	0.33	692	7999		

1

2 Boundary and loading conditions

3 Numerical simulations were performed using a dynamic quasi-static implicit analysis approach. Internal
4 pressures were applied on the blood vessel lumen and Vasa Vasorum to mimic the presence of blood flow. The
5 vessel's luminal pressure was set to 75.5 mmHg, which represents the average value of a pressure wave extracted
6 from patient-based coronary measurement (Rambhia et al. 2012). In the Vasa Vasorum a pressure of 15 mmHg
7 was chosen based on typical capillaries pressures ranges (Shore 2000). The stent was expanded with a uniform
8 and linearly increasing internal pressure up to an expansion ratio of 1.1:1. These pressures are 1.8, 1.6 and 1.6
9 MPa for stent A, stent B and stent C, respectively. The stent was then post-dilated by a higher pressure load
10 exerted on the central region of the stent, to achieve a ratio of 1.3:1 and minimize any dog-boning effect. The
11 post-dilation pressures are 2.2, 2 and 2 MPa for stent A, stent B and stent C respectively. This range of expanding
12 pressures agrees with those used in the clinical practice (Lanzer and Schmidt 2015). Nodes at the centre of
13 alternating stent vertices have been constrained to allow the device to move in the radial direction only. To
14 determine the effect of the alignment between the vertex and the space between vertices and the atheroma on the
15 numerical results, a cylindrical reference system was introduced and stent expansion tests were conducted with
16 the stent vertices aligned at 0 degrees position with the peak of the atheroma (stent vertices aligned with the
17 atheroma peak) and after rotating the stent by 30 degrees in the clockwise direction (stent valleys aligned with
18 the atheroma peak). The interaction between the device and the endothelium has the properties of "Hard" contact
19 for the normal behaviour and frictional sliding with a static friction coefficient of 0.15 for the tangential
20 behaviour, as previously used in (Schiavone, Zhao, and Abdel-Wahab 2014), (Karanasiou et al. 2013). The three
21 arterial layers are considered as bound together and free to deform in any direction. Lastly, the two axial extremes
22 of the artery are free to move in the radial direction only, reflecting the constraint from the artery to tissue
23 tethering.

24

25 Vasa Vasorum compression and change in flow resistance

26 After full expansion of each stent, we measured Vasa Vasorum deformations in VV1, VV2 and VV3, as
27 well as Top, Bottom, Left and Right locations, for VV segments in each vascular layer, and in both axial and
28 circumferential branches. Later, we calculated the increase in hydraulic resistance, taking into consideration that
29 after stenting the Vasa Vasorum cross-sections are no longer circular but elliptical, as shown in [Figure 2].
30 Therefore, the change in resistance to the flow was obtained using the formula for Poiseuille flow through a
31 straight tube of elliptical cross section (4) (Fraenkel 1971):

1
2
3
4
5
6
7

8
9
10
11
12
13
14
15
16
17
18
19
20
21
22

$$\frac{R_2}{R_1} = \frac{r^4(a^2+b^2)}{2(ab)^3}, \quad (7)$$

where R_2 and R_1 stand for the final and initial resistances to flow, respectively; r is the initial radius of the branch; a and b are the semi-major and semi-minor axes of the compressed Vasa, respectively. The acquired data are the diameters of the VV branches along the b-axis (minor-axis) in [Figure 2], at the proximity where the Vasa divide into the two circumferential Vasa. The amount of compression was evaluated as the radial change (along the b-axis in Figure 2) in distance between two point sets defining the extremity of the branch diameter. This was done using the XY Data post-processing tool in Abaqus and later implemented in a user-defined MATLAB code.

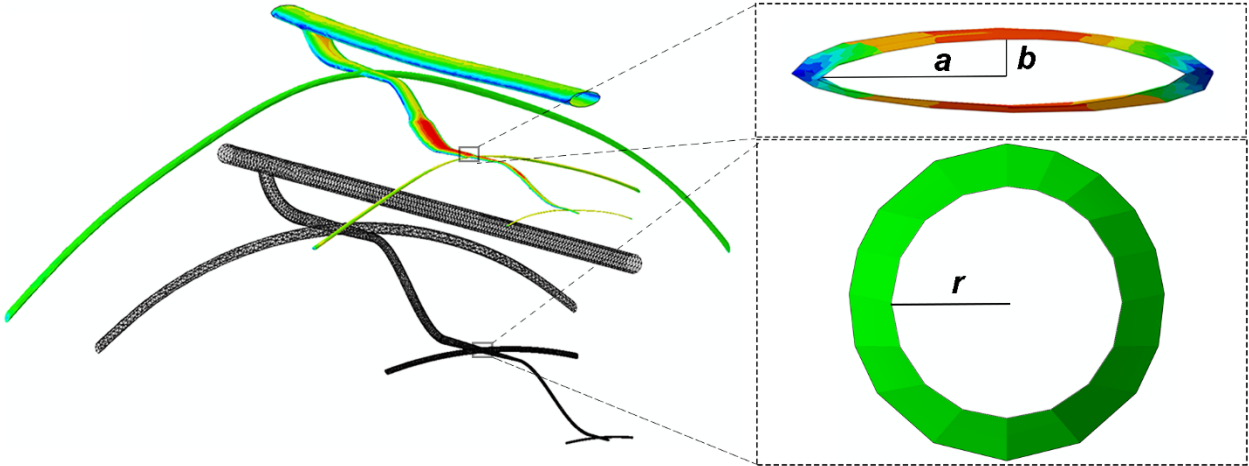
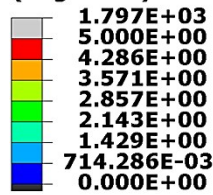


Figure 2. Illustration of the undeformed and deformed Vasa Vasorum branch, showing the circular (initial) cross-section of the vessel versus the elliptical (final) shape of the same region.

Results

Before collecting the data for VV compression, we analysed the stress and strain distribution on the arterial tissues induced by the stent designs at three expansion ratios [Figure 3]. First, the stent is expanded until reaching a stent/artery luminal diameter ratio of 1.1:1. Then, we replicate the post-dilation procedure, where the stent is expanded at a ratio of 1.2:1 and 1.3:1. The latter case is referred to as stent over-expansion. All three stents lead to a similar pattern of stresses (and strains), where the centre region of the artery has the highest stresses, and it exhibits most intense concentration in the region opposite to the lipid core. As expected, stresses increase as the stent is more dilated. In general, the strains also vary along the radial direction, being the highest in the luminal side of the artery, and decreasing inversely to the radius, thus resulting in lesser strains in the media and even lower in the adventitia.

S, Max. Principal
(Avg: 75%)

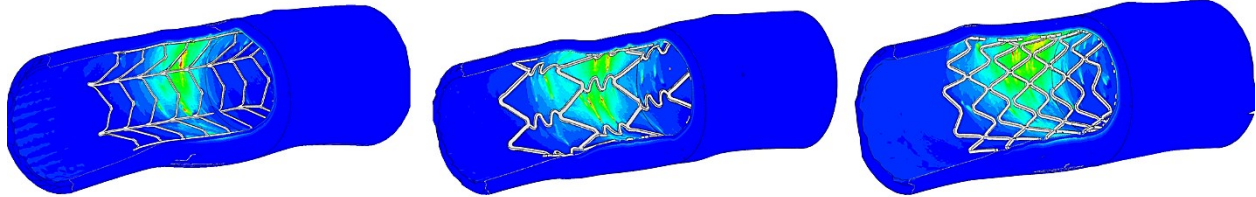


STENT A

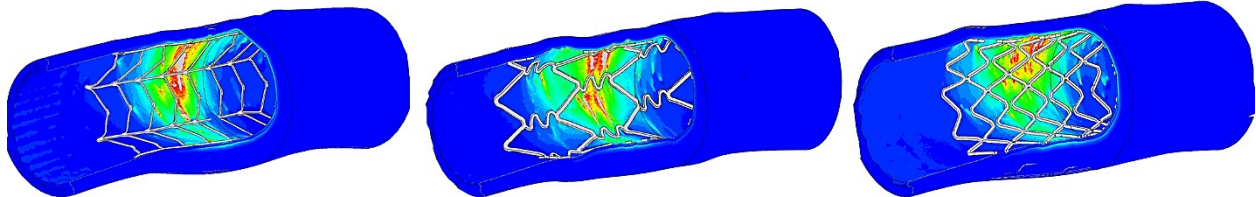
STENT B

STENT C

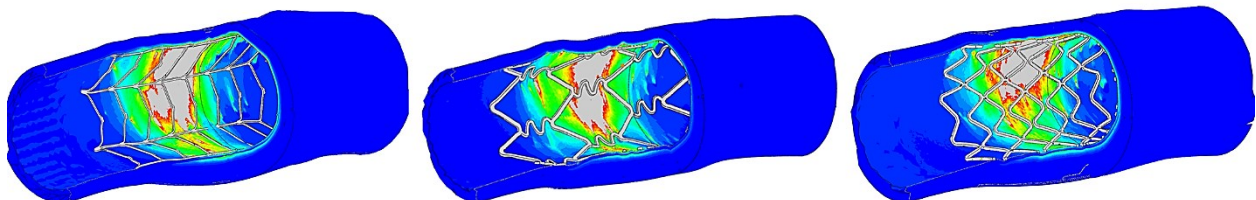
EXPANSION RATIO 1.1:1



EXPANSION RATIO 1.2:1



EXPANSION RATIO 1.3:1

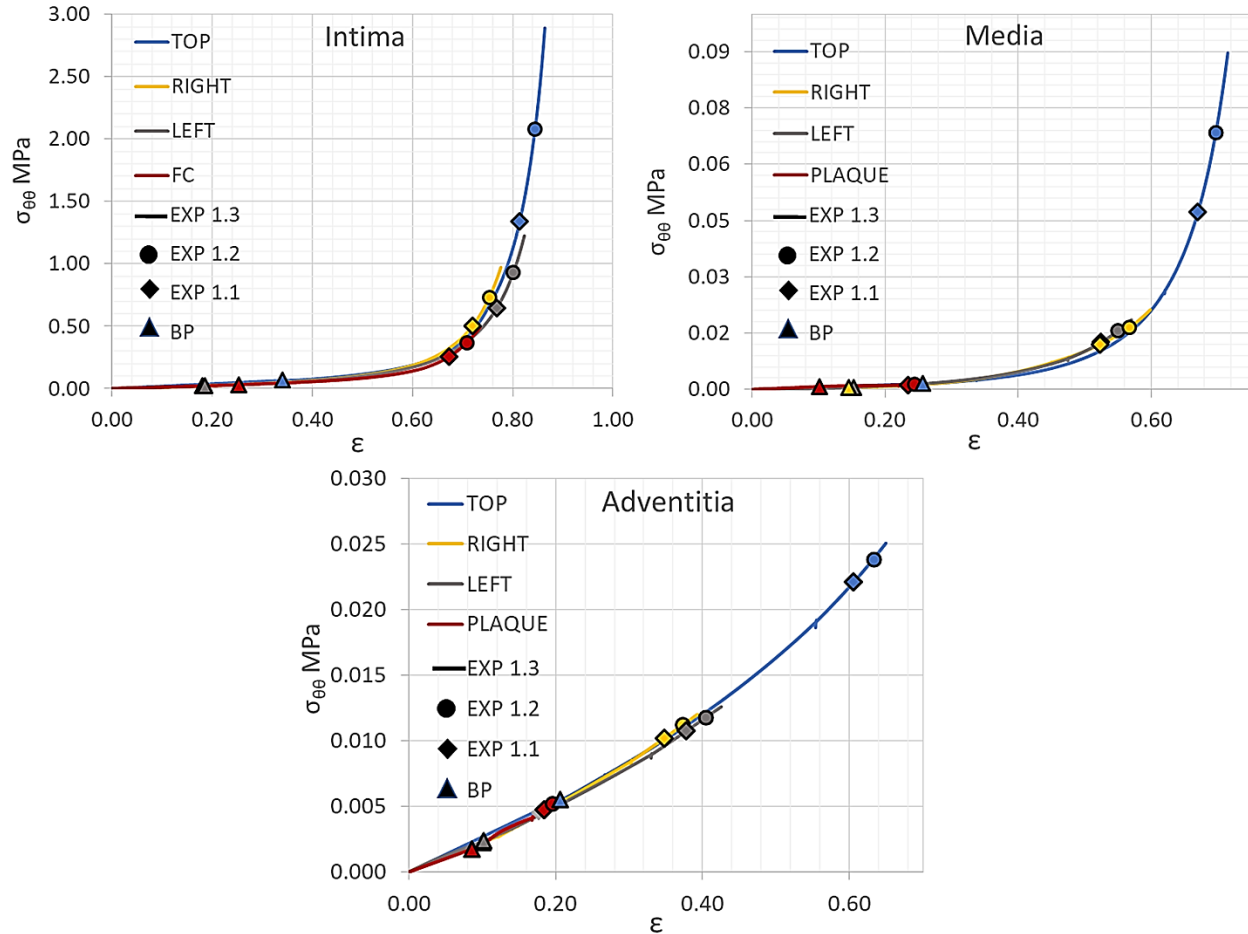


1

2 **Figure 3.** Representation of dilated artery (Max Principal stresses are reported in MPa) at three degrees of expansion for Stent A,
3 Stent B and Stent C.

4

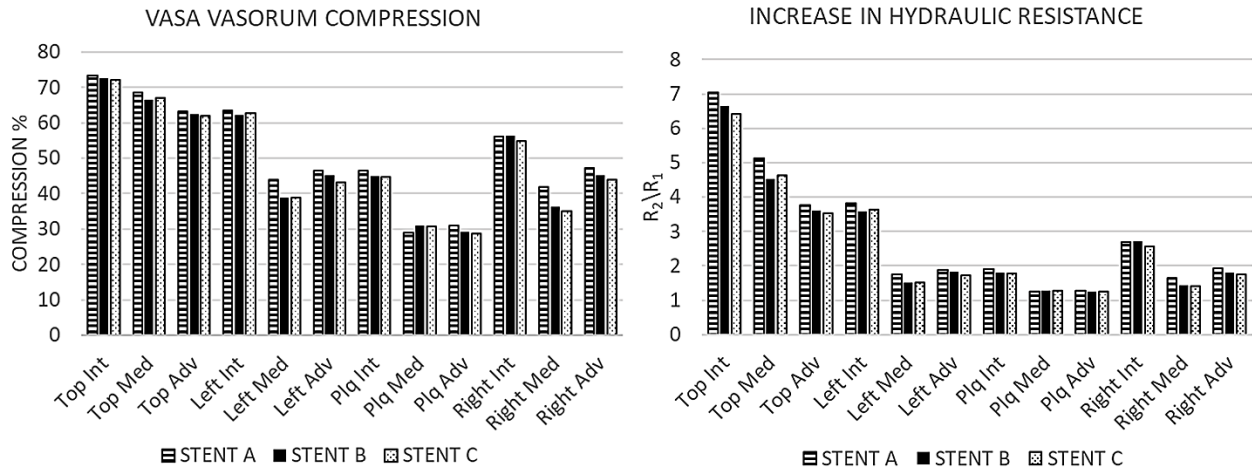
5 This behaviour is further described by the circumferential stress and strain curves in **[Figure 4]**, which
6 represents the average values of 30 mesh elements per curve that were selected along the radial thickness of each
7 layer at the middle of the artery in the longitudinal direction. Intima and Media exhibit the typical hyperelastic
8 response under high deformations, while Adventitia remains in the linear regime as highest stresses and strains
9 are sustained by the inner layers. Moreover, regions protected by the fibroatheroma experience the lowest
10 stresses and strains as shown for Media and Adventitia. The fibrous cap shows higher stresses with a peak
11 circumferential stress (PCS) that lies slightly below the average threshold for cap rupture (545 kPa (Cheng et al.
12 1993)). On the other hand, the region opposite to the stenosis undergoes major stresses and strains as well as the
13 highest pre-stretch due to the blood pressure. In general, the highest circumferential stresses occur on the Intima
14 and correspond to when the stent is overextended. Overall, these values agree with what has already been shown
15 by Schiavone et al. (Schiavone, Zhao, and Abdel-Wahab 2014).



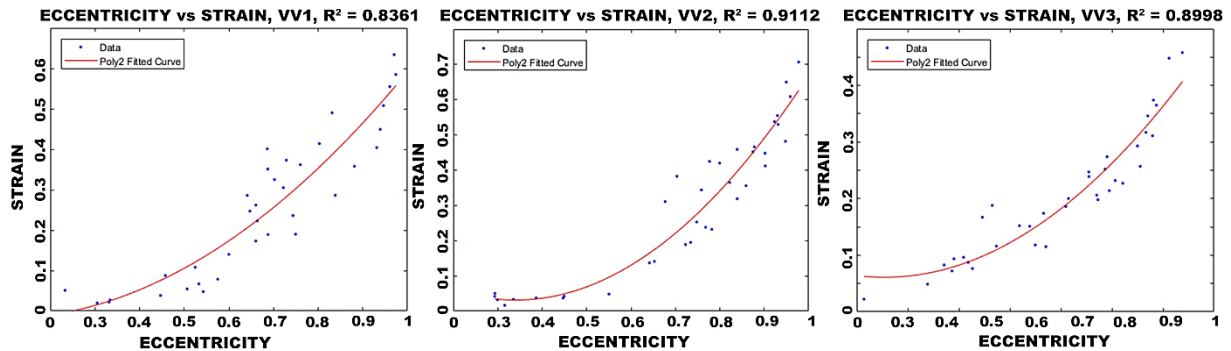
1 **Figure 4.** Circumferential Stresses vs. Strains exerted by Stent C for Intima, Media and Adventitia at each expansion ratio in
2 Top region, at the Right and Left sides, in the Fibrous Cap (intima) and under the Plaque (Media, Adventitia).

3 The VV compression and change in flow resistance due to blood pressure were calculated relative to the
4 initial undeformed configuration of the blood vessel, while for stenting, those measurements were obtained in
5 reference to the VV diameter under the blood pressure loaded configuration. Histograms for VV compression
6 and fold increase in flow resistance for the three stents are reported in **[Figure 5]**. The effect of the different
7 designs was compared for the case of overexpansion on the vasa VV2, which have always appeared to be the
8 most affected branches, given their location at the centre of the stenotic region (see **[Figure 1]**). Histograms refer
9 to central branches running longitudinally inside the vascular wall. Data for circumferential branches were also
10 analysed and showed no significant differences with central branches (data not shown). We found that when the
11 artery is expanded uniformly at a ratio of 1.3:1, the VV compression and increase in resistance to the blood flow
12 is similar among the three stents. On one hand, intraluminal pressure alone (relative to the initial undeformed
13 vessel configuration) produced a mild average compression of 12% on the VV2 network, with a maximum of
14 33% in the intimal-medial top region. In terms of resistance to blood flow, intraluminal pressure resulted in a
15 nearly null increase in resistance, with an average value of 1.07 and a maximum of 1.4. On the other hand, after
16 stenting, the branches on the opposite side of the stenosis are most impacted by the stent expansion, with the
17 highest compressions observed among the VV, which range between 69-75% in Media and Intima. These levels
18 of deformation lead to hydraulic resistances that are five to eight times higher than in a physiological condition.
19 In contrast, branches beneath the plaque experience a minimal change in the radial axis (b dimension) as well as
20 change in flow resistance. These results highlight the shielding behaviour of the plaque which protects the vasa
21 underneath it. The pattern of vasa disruption reflects the stress and strain distributions in the artery. As a matter

1 of fact, Vasa Vasorum deformation is strongly correlated with the strain levels of the arterial tissues as depicted
 2 in [Figure 6]. Here, the eccentricity of the VV cross-sections, i.e., how much the branch is compressed, shows
 3 strong polynomial correlations with the vascular wall deformation. Overall, the VV compression after stenting
 4 (exp1.3) are at least twice and up to seven times higher than the compression produced by blood pressure alone,
 5 leading to one to seven fold increase in hydraulic resistance in the VV.
 6
 7



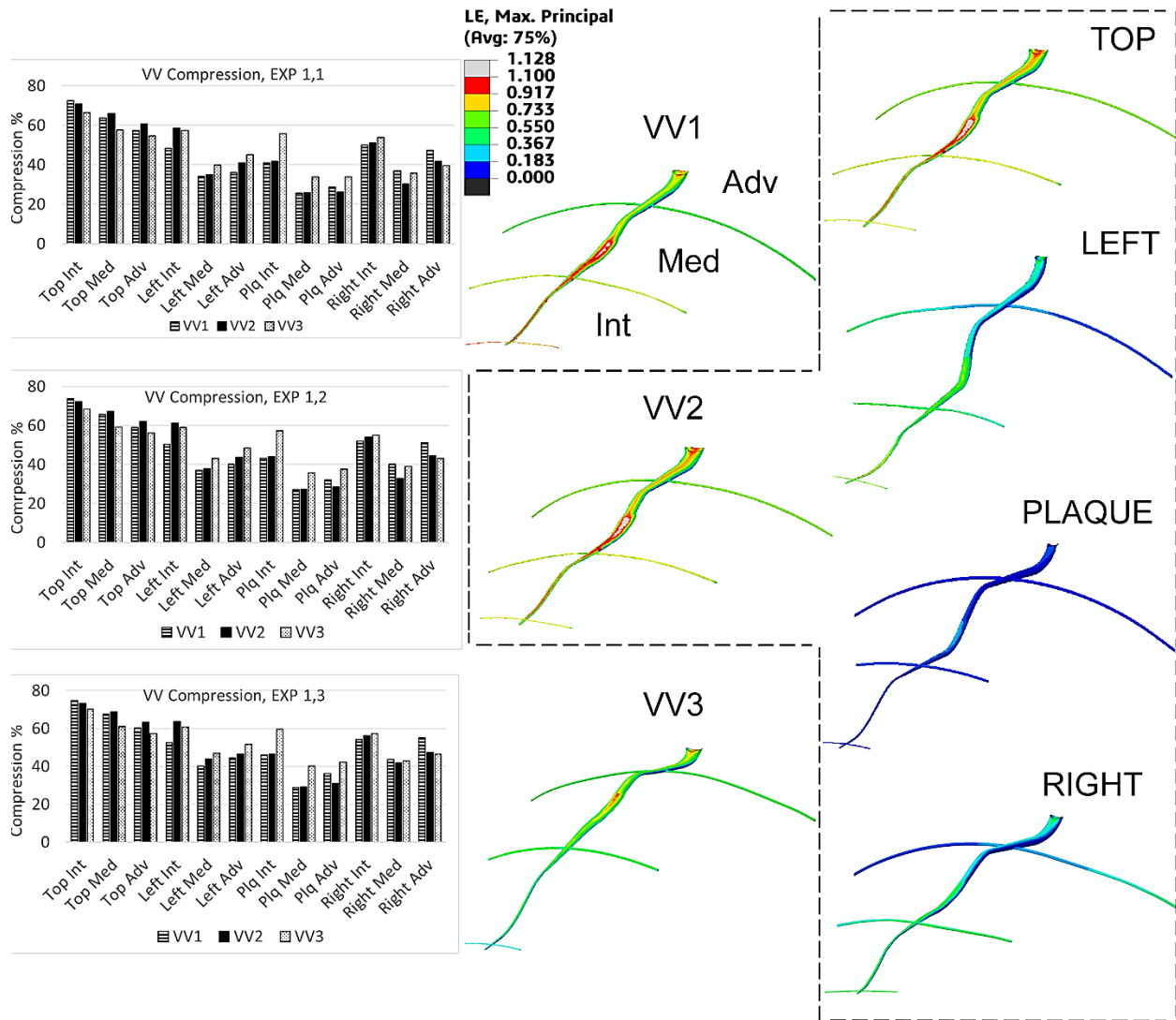
8
 9 **Figure 5.** Histograms of compression (left) and increase in hydraulic resistance (right) in VV2, caused by Stent A, B, C at 1.3:1
 10 expansion ratio.
 11



12
 13 **Figure 6.** Polynomial correlation between eccentricity (defined as $\epsilon = \sqrt{1 - \frac{b^2}{a^2}}$) of the VV cross section after expansion and
 14 the corresponding strain levels in the arterial layers for VV1, VV2 and VV3. Here, the data of the three layers Intima, Media and
 15 Adventitia were considered together in the same graph for the respective VV.
 16

17 Compression and change in resistance to flow for the entire vasa network at each expansion ratio are reported
 18 for Stent A only [Figure 7], since the three stent designs didn't show significant differences in the results. Again
 19 we found that the central branches on the opposite side of the stenosis are the most deformed by the angioplasty
 20 procedure. Intimal and medial Vasa reach a maximum of about 70-75% radial compression in the VV1 and VV2
 21 networks. Beneath the lipid core, Vasa Vasorum experience minimum compressions. The intimal VV3 branch
 22 close to the stenotic region shows higher compression levels as it is not shielded by the plaque (see [Figure 1]).
 23 Overall, the branches that belong to Vasa Vasorum 2 undergo the highest levels of deformation [Figure 7]. This

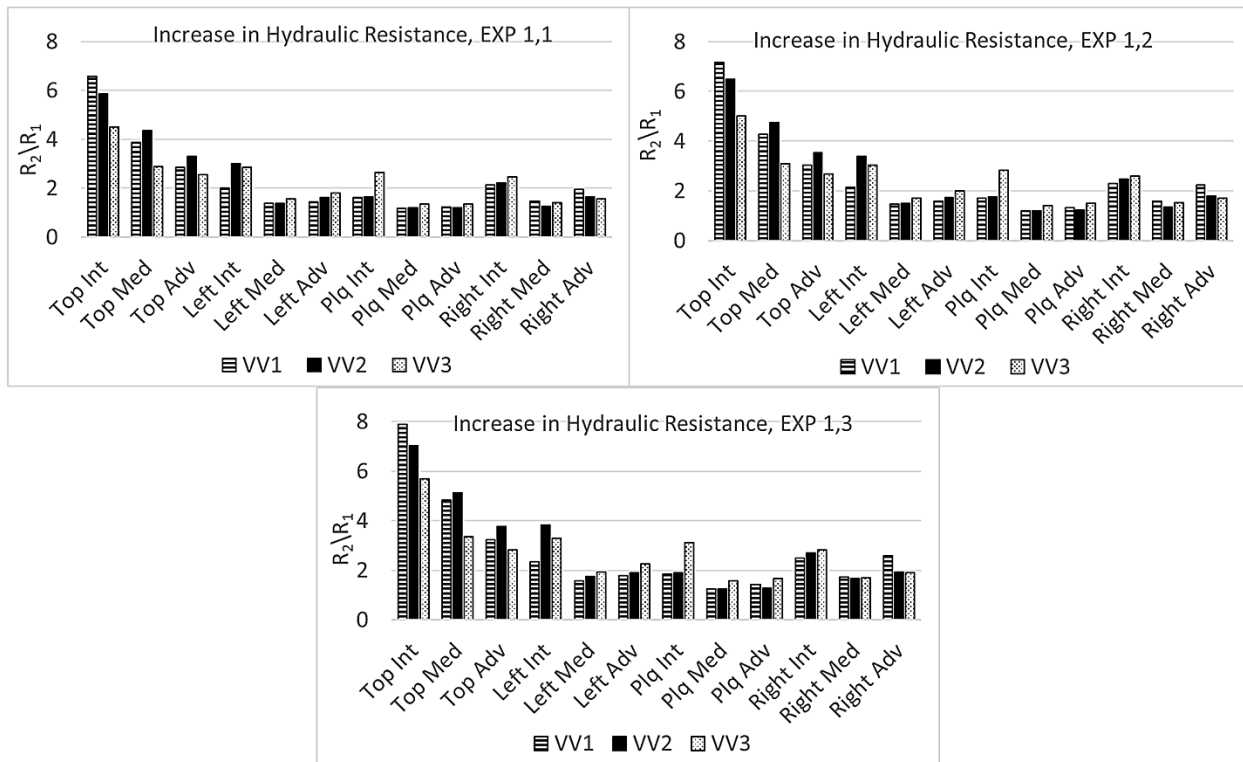
1 can also be seen in the strain distribution along the vasa branches [Figure 7] where the medial and intimal VV2
 2 in the top region experience the highest deformation. After rotating the stent by 30 degrees in the circumferential
 3 direction, the compression values for VV2 were 0.5% lower on average.
 4



5
 6 **Figure 7.** Left: Histograms of radial compression in VV1, VV2 and VV3 for Intima, Media and Adventitia at the four cross-
 7 sectional regions after the three stent expansions. Centre: Strain distribution on VV1, VV2 and VV3 branches running in the
 8 region opposite to the lipid core, at 1.3:1 expansion ratio. Right: Strain distribution on VV2 vasa branches on the top – opposite
 9 side of the stenosis -, on the left, under the stenotic plaque, and on the right side, at 1.3:1 expansion ratio. The left, right and
 10 under the plaque branches were rotated to the same orientation as the top branch for clarity.

11
 12 The results for the fold change in hydraulic resistance are presented in [Figure 8]. The resistance to the flow
 13 in central branches changes in a similar manner as the radial compression. Top branches in the VV1 and VV2
 14 reach the greatest fold increase, where the resistance to the flow is 5-8 times higher when the stent is over
 15 expanded. Our results indicate that Vasa Vasorum blood flow would be disrupted the most in the Media and
 16 Intima layers. The flow reduction could potentially be even greater reduction in branches that are connected in-
 17 series with upstream vasa. Overall, the maximum increase in flow resistance happens under a stent/artery luminal

1 diameter ratio of 1.3:1. After rotating the stent by 30 degrees in the circumferential direction, the change in flow
 2 resistance for VV2 was 1.27% lower on average.
 3



4
 5 **Figure 8.** Histograms of fold change in resistance to the blood flow in VV1, VV2 and VV3 (A-C) central branches for Intima,
 6 Media and Adventitia at the four layers regions after the three stent expansions (Stent A)

7
 8

9 **Discussion**

10 In the present study, we investigated the effects of stent deployment on arterial Vasa Vasorum
 11 deformation and the consequent changes on resistance to blood flow, under different degrees of expansion.
 12 We also considered three commonly used stent designs to determine whether VV disruption changes
 13 depending on the stent layout. Previous studies of Vasa Vasorum have focused their attention primarily on
 14 their morphology and the relationship between Vasa neovascularization and plaque progression (Baikoussis
 15 et al. 2011; Cabello et al. 2010; Chiefari et al. 2006; Gössl et al. 2015; Heistad, Armstrong, and Amundsen
 16 2017; T. G. Kwon, Lerman, and Lerman 2015; Mulligan-Kehoe 2009; Patzelt et al. 2019; Taruya et al.
 17 2015; Zorc-Pleskovič et al. 2018). On the other hand, the literature is rich in Finite Element analyses that
 18 investigated the biomechanical interactions between stents and the vascular wall. Hajiali *et al.* (Hajiali et
 19 al. 2015) analysed the stresses induced by stenting in an idealized multi-layered atherosclerotic coronary
 20 artery model. Similar to the current study, the authors obtained low wall stress levels beneath the plaque,

1 suggesting the shielding behaviour of the atheroma. In another paper, Zehedmanesh *et al.* (Zahedmanesh
2 and John 2010) investigated the importance of considering the balloon geometry when simulating stent
3 expansion. In our study, the wall stress distributions don't display significant differences with the results
4 obtained by these previous studies when taking into account the presence of the balloon. Our results also
5 agree with those presented by Zehedmanesh *et al.* (Zahedmanesh and Lally 2009) who analysed the effects
6 of thin stent struts on the arterial tissue. Moreover, they observed that Von Misses stress peak values more
7 than doubled when increasing stent expansion, an outcome that is replicated in our simulations, even if our
8 model includes an anisotropic description of the arterial tissues. In addition, Karimi *et al.* (Karimi,
9 Navidbakhsh, and Razaghi 2014) assessed the plaque and arterial wall vulnerability after stent expansion.
10 In agreement with our study, the authors reported that the highest stresses were located in the Intima, the
11 stiffest layer of the vascular wall.

12 In the current study, we have looked further to assess how the vascular wall stresses and strains affect
13 the Vasa Vasorum. In particular, we have found that stent expansion leads to varying degrees of Vasa
14 compression and an overall increase in the resistance to blood flow. These structural changes depend on
15 the Vasa location within the arterial wall and the amount of stent expansion. First, we observed that the
16 highest VV deformations occur on the opposite side of the plaque, where medial and intimal Vasa reach a
17 final minor-axis (b-axis) of 7 μm (70% compression) and 1 μm (75% compression), respectively. On the
18 other hand, the lowest Vasa compressions are beneath the atheroma, which appears to shield the tissue
19 underneath it, taking up most of the stress. These results can be explained by the fact that the plaque exerts
20 higher resistance to expansion than the non-atherosclerotic regions. Therefore, the stent dilates non-
21 homogeneously, expanding and stretching the arterial tissues across from and to the side of the plaque
22 differently. Hajiali *et al.* . (Hajiali et al. 2015) reported that stresses in the arterial wall behind the plaque
23 are inversely correlated with the degree of stenosis. Their results suggest that thinner plaques would expose
24 the tissues underneath them to higher stresses leading to greater VV deformations in the stenotic region. In
25 this study, we have considered a generalized atherosclerotic plaque that causes 60% stenosis which
26 represents a common situation when stenting is required. The levels of VV compression and resistance to
27 flow likely depend on the tissues material properties as well. In this regard, Iannaccone et al. (Iannaccone
28 et al. 2014) reported higher stresses in the Media underlying hard, calcified plaques. In another extensive
29 study, Akyildiz et al. (Akyildiz et al. 2011) described the effect of Intima stiffness on the stress distributions
30 in stenotic arteries. In particular, a soft material description of the Intima leads to a greater contribution of
31 the outer layers in supporting the overall load. Therefore, in the case of calcified plaques and less stiff
32 intimal tissue we would expect higher deformations in the medial and adventitial Vasa Vasorum. The trend
33 of vasa network disruption appears to hold true regardless of the stent design, as different stents show highly
34 similar results. Moreover, the distribution of Vasa deformation doesn't change depending on the
35 circumferential orientation of the stent structure, which has a minor effect on the levels of disruption.

36 The second important finding of our study is the major effect on VV in the Medial layer. Here, there
37 appear to be relevant compressions for central branches, with a resistance to the blood flow as much as 5
38 times as high as in the healthy condition under stent overexpansion (both 1.2:1 and 1.3:1). Even for normal
39 expansions of 1.1:1, resistances to blood flow may be increased by almost 4.5 – fold. If we consider the
40 overall Vasa organization to have an “in series” characteristic, then it is likely that the net increase in overall
41 resistance would greatly exceed 6. Furthermore, it is worth noting that in cases of highest compression, the
42 radial dimension (minor axes) of the Vasa could be smaller than 2.7 μm , completely preventing red blood
43 cells from passing through that region (George A., Fan, and David F. 2004).

1 A limitation intrinsic to numerical studies using idealized geometries is the fact that real morphology
2 of the blood vessel, atheroma and vasa vasorum are much more complex, and may not be fully captured by
3 the model. On the other hand, models are used to simplify very complex problems that may otherwise be
4 intractable. We have made an effort to perform a quantitative analysis of changes in VV compression and
5 flow resistance due to stent overexpansion in what is considered a typical atheroma with 60% stenosis. The
6 VV tree was designed so that both axial and circumferential branches within the three layers of the blood
7 vessel, and within different axial locations were considered in the analysis. However, this analysis is not
8 exhaustive in that other degrees of stenosis and range of tissue properties are not considered here, and
9 warrant to be investigated in future work. Nowadays, this is a first report demonstrating the significant role
10 (fold change) on VV compression and reduction of flow resistance due to stent overexpansion.

11 Previous papers have highlighted the negative consequences that reduction of Vasa Vasorum blood
12 flow causes in the Medial layer. Sanada *et al.* (Sanada et al. 1998) have reported medial atrophy after stent
13 deployment in dogs, with consequent intimal hyperplasia (IH) and VV proliferation, probably due to
14 hypoxia in the arterial wall. Moreover, Kantor *et al.* (Kantor and Möhlenkamp 2003) demonstrated medial
15 hypoxia in porcine coronary arteries after stenting, throughout the 28 day study period, by means of
16 immunohistochemistry with the hypoxia marker pimonidazol. Using in-vivo blood-flow measurements, the
17 authors suggested significant VV compression leading to an absolute cessation of VV blood flow. Then,
18 Santilli *et al.* (Santilli, Tretinyak, and Lee 2000) mapped the oxygen tension levels in the artery wall of
19 rabbits under different degrees of stent expansion. The results showed the lowest oxygen concentrations
20 located in the Media as well as a correlation between hypoxia and the stent final diameter. The latter
21 relationship is also clear in our results. In fact, Vasa Vasorum deformations increase with stent expansion,
22 reaching severe compressions and resistances to flow when the stent is over-expanded. Stent over-
23 expansion induces higher stresses and strains on the vascular wall, increasing the chance of tissue damage
24 and, as we are showing, decreasing Vasa Vasorum blood flow. Arterial wall injury and hypoxia are well
25 known precursors of neointimal hyperplasia. Timmins *et al.* (Timmins et al. 2011) demonstrated that higher
26 vascular wall stresses after stenting correlates with thicker neointimal formation in pigs. Along the same
27 lines, Russo *et al.* (Russo, Silva, and Yeager 2007) and Mitsutake et al. (Mitsutake et al. 2017) showed that
28 neointimal proliferation and hyperplasia in pigs are strongly associated with increasing stent-artery
29 diameter ratio. As our results show, higher Vasa Vasorum compressions due to stent over-expansion could
30 be the underlying cause of IH development. This situation will be experienced the most in the healthy region
31 of the artery and it could trigger the excessive inflammatory response that would result in neointimal
32 hyperplasia. Histological inspections of in-stent restenosis (Alfonso et al. 2014; Mori et al. 2017; Soga,
33 Inoue, and Kuma 2015; Yeh, Oh, and Hsueh 2016) show that NH forms all around the stent structure,
34 resulting in nearly uniform new narrowing of the stented area. However, thicker regions of neointimal tissue
35 can occur and have been previously related to the degree of injury of the internal elastic lamina IEL (Gunn
36 et al. 2002). Since deeper damage to intimal tissue is related to high stretching and stresses caused by the
37 stent, it is possible that the Vasa Vasorum network that perfuses the same region is being deformed
38 excessively, exposing the tissue to hypoxia. However, to our knowledge the morphology and spatial growth
39 of intimal hyperplasia have not been compared against different degrees of wall hypoxia and certainly
40 warrant to be investigated in future studies. In conclusion, it has been demonstrated that stent-
41 overexpansion to enlarge the lumen is a counterproductive strategy and entails a greater chance of IH
42 formation. This reaction is likely the result of arterial tissue injury, including wall hypoxia caused by Vasa
43 Vasorum compression.

1

2 **Data accessibility**

3 This article has no additional data

4 **Competing Interest**

5 The authors have no competing interest to declare.

6

7 **Authors' Contribution**

8 *AC carried out the design of numerical model, performed numerical simulations, gathered data and*
9 *carried out data analysis, participated in the design of the study and drafted the manuscript; ADP participated*
10 *in the design of numerical model, development and supervision of numerical simulations and critically revised*
11 *the manuscript; JT conceived of the study, designed the study, coordinated the study, helped draft and revise*
12 *the manuscript, LC designed the study, coordinated the study, helped draft and revise the manuscript. All*
13 *authors gave final approval for publication and agree to be held accountable for the work performed therein.*

References

- Akyildiz, Ali C. et al. 2011. "Effects of Intima Stiffness and Plaque Morphology on Peak Cap Stress." *BioMedical Engineering Online* 10(1): 25.
- Alfonso, Fernando, Robert A. Byrne, Fernando Rivero, and Adnan Kastrati. 2014. "Current Treatment of In-Stent Restenosis." *Journal of the American College of Cardiology* 63(24): 2659–73.
- Baikoussis, Nikolaos G. et al. 2011. "The Implication of Vasa Vasorum in Surgical Diseases of the Aorta." *European Journal of Cardio-thoracic Surgery* 40(2): 412–17.
- Benjamin, Emelia J. et al. 2018. 137 *Circulation Heart Disease and Stroke Statistics - 2018 Update: A Report from the American Heart Association*.
- . 2019. 139 *Circulation Heart Disease and Stroke Statistics—2019 Update: A Report From the American Heart Association*. <https://www.ahajournals.org/doi/10.1161/CIR.0000000000000659>.
- Cabello, Christopher M et al. 2010. "Prevention of Vasa Vasorum Neovascularization Attenuates Early Neointima Formation in Experimental Hypercholesterolemia." *NIH* 46(2): 220–31.
- Cardoso, L., Kelly-Arnold, A., Maldonado, N., Laudier, D., & Weinbaum, S. 2014. "Effect of Tissue Properties, Shape and Orientation of Microcalcifications on Vulnerable Cap Stability Using Different Hyperelastic Constitutive Models." *Journal of Biomechanics* 47(4): 870–77.
- Caro, Colin Gerald et al. 2013. "Intimal Hyperplasia Following Implantation of Helical-Centreline and Straight-Centreline Stents in Common Carotid Arteries in Healthy Pigs: Influence of Intraluminal Flow." *Journal of the Royal Society Interface* 10(89): 1–8.
- Cheema, Asim N et al. 2006. "Adventitial Microvessel Formation After Coronary Stenting and the Effects of SU11218 , a Tyrosine Kinase Inhibitor." 47(5).
- Cheng, G. C. et al. 1993. "Distribution of Circumferential Stress in Ruptured and Stable Atherosclerotic Lesions: A Structural Analysis with Histopathological Correlation." *Circulation* 87(4): 1179–87.
- Chiefari, John et al. 2006. "Vasa Vasorum and Atherosclerosis –Quid Novi?" *American Chemical Society, Polymer Preprints, Division of Polymer Chemistry* 40(2): 344–45.
- Fraenkel, L. E. 1971. "Theoretical Hydrodynamics." *Journal of Fluid Mechanics* 45(3): 622–24.
- Fratzl, Peter. 2008. *Collagen: Structure and Mechanics, an Introduction*. ed. Peter Fratzl. Boston, MA: Springer.
- Fröbert, Ole et al. 2013. "Effect of Stent Inflation Pressure and Post-Dilatation on the Outcome of Coronary Artery Intervention. A Report of More than 90 000 Stent Implantations." *PLoS ONE* 8(2): 1–10.
- Gasser, T. Christian, Ray W. Ogden, and Gerhard A. Holzapfel. 2006. "Hyperelastic Modelling of Arterial Layers with Distributed Collagen Fibre Orientations." *Journal of the Royal Society Interface* 3(6): 15–35.
- George A., Truskey, Yuan Fan, and Katz David F. 2004. "Transport Phenomena in Biological Systems-Prentice Hall (2004)."
- Gössl, M. et al. 2015. "Impact of Coronary Vasa Vasorum Functional Structure on Coronary Vessel Wall Perfusion Distribution." *American Journal of Physiology-Heart and Circulatory Physiology* 285(5): H2019–26.
- Gunn, Julian et al. 2002. "Coronary Artery Stretch versus Deep Injury in the Development of In-Stent Neointima." *Heart* 88(4): 401–5.
- Hajjali, Zuned et al. 2015. "Tissue Prolapse and Stresses in Stented Coronary Arteries: A Computer Model for Multi-Layer Atherosclerotic Plaque." *Computers in Biology and Medicine* 66: 39–46. <http://dx.doi.org/10.1016/j.compbiomed.2015.08.014>.
- He, R. et al. 2020. "Finite Element Evaluation of Artery Damage in Deployment of Polymeric Stent with Pre- and

- Post-Dilation.” *Biomechanics and Modeling in Mechanobiology* 19(1): 47–60.
- Heistad, D. D., M. L. Armstrong, and S. Amundsen. 2017. “Blood Flow through Vasa Vasorum in Arteries and Veins: Effects of Luminal PO₂.” *American Journal of Physiology-Heart and Circulatory Physiology* 250(3): H434–42.
- Holzapfel, Gerhard. 2002. “Nonlinear Solid Mechanics: A Continuum Approach for Engineering Science.” *Meccanica* 37(4/5): 489–90.
- Iannaccone, F. et al. 2014. “The Influence of Vascular Anatomy on Carotid Artery Stenting: A Parametric Study for Damage Assessment.” *Journal of Biomechanics* 47(4): 890–98.
- Kantor, Birgit, and Stefan Möhlenkamp. 2003. “Imaging of Myocardial Microvasculature Using Fast Computed Tomography and Three-Dimensional Microscopic Computed Tomography.” *Cardiology Clinics* 21(4): 587–605.
- Karanasiou, Georgia S. et al. 2013. “Modeling Stent Deployment in Realistic Arterial Segment Geometries: The Effect of the Plaque Composition.” *13th IEEE International Conference on BioInformatics and BioEngineering, IEEE BIBE 2013*: 18–21.
- Karimi, Alireza, Mahdi Navidbakhsh, Mansour Alizadeh, and Ahmad Shojaei. 2014. “A Comparative Study on the Mechanical Properties of the Umbilical Vein and Umbilical Artery under Uniaxial Loading.” *Artery Research* 8(2): 51–56.
- Karimi, Alireza, Mahdi Navidbakhsh, and Reza Razaghi. 2014. “A Finite Element Study of Balloon Expandable Stent for Plaque and Arterial Wall Vulnerability Assessment.” *Journal of Applied Physics* 116(4).
- Kwon, Hyuck Moon et al. 1998. “Adventitial Vasa Vasorum in Balloon-Injured Coronary Arteries: Visualization and Quantitation by a Microscopic Three-Dimensional Computed Tomography Technique.” *Journal of the American College of Cardiology* 32(7): 2072–79.
- Kwon, Taek Geun, Lilach O. Lerman, and Amir Lerman. 2015. “The Vasa Vasorum in Atherosclerosis: The Vessel within the Vascular Wall.” *Journal of the American College of Cardiology* 65(23): 2478–80.
- L. Ritman, A. Lerman, Author. 2008. “The Dynamic Vasa Vasorum.” *Cardiovasc Res* 75(4): 649–58.
- Lally, C., A. J. Reid, and Patrick J. Prendergast. 2004. “Elastic Behavior of Porcine Coronary Artery Tissue under Uniaxial and Equibiaxial Tension.” *Annals of Biomedical Engineering* 32(10): 1355–64.
- Lanzer, Peter, and Wolfram Schmidt. 2015. “Instrumentation for Coronary Artery Interventions BT - PanVascular Medicine.” In ed. Peter Lanzer. Berlin, Heidelberg: Springer Berlin Heidelberg, 1979–2027. https://doi.org/10.1007/978-3-642-37078-6_67.
- Meads, C et al. 2000. “Rapid Review Coronary Artery Stents in the Treatment of Ischaemic Heart Disease : Standing Group on Health Technology Chair :” 4(23).
- Mitsutake, Yoshiaki et al. 2017. “Differences in Vascular Response between Balloon Overstretch and Stent Overexpansion in Nonatherosclerotic Porcine Coronary Arteries.” *Comparative medicine* 67(4): 350–55. <http://www.ncbi.nlm.nih.gov/pubmed/28830582><http://www.pubmedcentral.nih.gov/articlerender.fcgi?artid=PMC5557207>.
- Mori, Hiroyoshi et al. 2017. “Pathology of Chronic Total Occlusion in Bare-Metal Versus Drug-Eluting Stents: Implications for Revascularization.” *JACC: Cardiovascular Interventions* 10(4): 367–78. <http://dx.doi.org/10.1016/j.jcin.2016.11.005>.
- Mulligan-Kehoe, Mary Jo. 2009. “The Vasa Vasorum in Diseased and Nondiseased Arteries.” *American Journal of Physiology-Heart and Circulatory Physiology* 298(2): H295–305.
- Murphy, Eoin A., Adrian S. Dunne, David M. Martin, and Fergal J. Boyle. 2016. “Oxygen Mass Transport in Stented Coronary Arteries.” *Annals of Biomedical Engineering* 44(2): 508–22.

- Patzelt, Matej et al. 2019. "Morphology of the Vasa Vasorum in Coronary Arteries of the Porcine Heart: A New Insight." *Annals of Anatomy* 223: 119–26. <https://doi.org/10.1016/j.aanat.2019.02.006>.
- Pels, Klaus, Marino Labinaz, Cyrla Hoffert, and Edward R O'Brien. 1999. "Adventitial Angiogenesis Early After Coronary Angioplasty Correlation With Arterial Remodeling." *Arterioscler Thromb Vasc Biol.*
- de Quadros, Alexandre Schaan et al. 2006. "Hyperexpansion of Coronary Stents and Clinical Outcomes." *Texas Heart Institute journal / from the Texas Heart Institute of St. Luke's Episcopal Hospital, Texas Children's Hospital* 33(4): 437–44.
- Rambhia, S. H. et al. 2012. "Microcalcifications Increase Coronary Vulnerable Plaque Rupture Potential: A Patient-Based Micro-Ct Fluid-Structure Interaction Study." *Annals of Biomedical Engineering* 40(7): 1443–54.
- Ritman, E. L., and A. Leman. 2008. "The Dynamic of Vasa Vasorum." *Cardiovasc Res* 6(4): 247–53.
- Russo, Robert J., Patricia D. Silva, and Mark Yeager. 2007. "Coronary Artery Overexpansion Increases Neointimal Hyperplasia after Stent Placement in a Porcine Model." *Heart* 93(12): 1609–15.
- Sanada, Jun-ichiro, Osamu Matsui, Jun Yoshikawa, and Toshihiko Matsuoka. 1998. "Cardio Vascular and Interventional Radiology An Experimental Study of Endovascular Stenting with Special Reference to the Effects on the Aortic Vasa Vasorum." 0031: 45–49.
- Santilli, S M, A S Tretinyak, and E S Lee. 2000. "Transarterial Wall Oxygen Gradients at the Deployment Site of an Intra- Arterial Stent in the Rabbit." *Am J Physiol Heart Circ Physiol* 279(4): H1518-25.
- Schiavone, A., L. G. Zhao, and A. A. Abdel-Wahab. 2014. "Effects of Material, Coating, Design and Plaque Composition on Stent Deployment inside a Stenotic Artery - Finite Element Simulation." *Materials Science and Engineering C* 42: 479–88.
- Shit, J, S Dhar, and S Acharyya. 2013. "Characterization of Cyclic Plastic Behavior of SS 316 Stainless Steel." *International Journal of Engineering Science and Innovative Technology (IJESIT)* 2(5): 524–38.
- Shore, Angela C. 2000. "Capillaroscopy and the Measurement of Capillary Pressure." *J Clin Pharmacol* 50: 501–13.
- Soga, Yoshimitsu, Katsumi Inoue, and Sosei Kuma. 2015. "Pathological Findings of Late Stent Thrombosis after Paclitaxel-Eluting Stent Implantation for Superficial Femoral Artery Disease." *Journal of Cardiology Cases* 11(2): 39–41. <http://dx.doi.org/10.1016/j.jccase.2014.10.002>.
- Tarbell, John et al. 2020. "The Role of Oxygen Transport in Atherosclerosis and Vascular Disease." *Journal of The Royal Society Interface* 17(165): 20190732.
- Taruya, Akira et al. 2015. "Vasa Vasorum Restructuring in Human Atherosclerotic Plaque Vulnerability: A Clinical Optical Coherence Tomography Study." *Journal of the American College of Cardiology* 65(23): 2469–77.
- Timmins, Lucas H., Matthew W. Miller, Fred J. Clubb Jr., and James E. Moore Jr. 2011. "Increased Artery Wall Stress Post-Stenting Leads To Greater Intimal Thickening." *HHS Public Access* 91(6): 955–67.
- Tretinyak, Alexander S. et al. 2002. "Supplemental Oxygen Reduces Intimal Hyperplasia after Intraarterial Stenting in the Rabbit." *Journal of Vascular Surgery* 35(5): 982–87.
- Vasuri, Francesco et al. 2012. "Nestin and WT1 Expression in Small-Sized Vasa Vasorum from Human Normal Arteries." *Histology and Histopathology* 27: 1195–1202.
- Williams, J K, and D D Heistad. 1996. "Structure and Function of Vasa Vasorum." *Trends in cardiovascular medicine* 6(2): 53–57.
- Yeh, Jong Shiuan, Seung Jin Oh, and Chun Mei Hsueh. 2016. "Frequency of Vascular Inflammation and Impact on Neointimal Proliferation of Drug Eluting Stents in Porcine Coronary Arteries." *Acta Cardiologica Sinica* 32(5): 570–77.
- Zahedmanesh, Houman, and Daniel John. 2010. "Simulation of a Balloon Expandable Stent in a Realistic Coronary Artery — Determination of the Optimum Modelling Strategy." 43: 2126–32.

- Zahedmanesh, Houman, and Caitríona Lally. 2009. "Determination of the Influence of Stent Strut Thickness Using the Finite Element Method: Implications for Vascular Injury and in-Stent Restenosis." *Medical and Biological Engineering and Computing* 47(4): 385–93.
- Zhang, Z-J et al. 2010. "Differential Effects of Post-Dilation after Stent Deployment in Patients Presenting with and without Acute Myocardial Infarction." *Am Heart J.* 160(5): 979–86.
- Zorc-Pleskovič, Ruda et al. 2018. "Immune Cells and Vasa Vasorum in the Tunica Media of Atherosclerotic Coronary Arteries." *Bosnian Journal of Basic Medical Sciences* 18(3): 240–45.